RESEARCH ARTICLE

Diffusion kurtosis imaging of microstructural changes in brain tissue affected by acute ischemic stroke in different locations

Liu-Hong Zhu[1,2], **Zhong-Ping Zhang**[3], **Fu-Nan Wang**[1], **Qi-Hua Cheng**[1], **Gang Guo**[1,*]
1 Department of Radiology, Xiamen Second Hospital, Xiamen, Fujian Province, China
2 Department of Radiology, Xiamen Branch, Zhongshan Hospital, Fudan University, Xiamen, Fujian Province, China
3 MR Research China, GE Healthcare, Beijing, China

Funding: *This study was supported by the Science and Technology Planned Project from Xiamen Science and Technology Bureau, China, No. 3502Z20154065 (to LHZ); the Joint Project for Xiamen Key Diseases from Xiamen Science and Technology Bureau, China, No. 3502Z20149032 (to GG).*

Graphical Abstract

Performance of diffusion kurtosis imaging (DKI) in detecting the microstructure changes at different locations of the brain after acute ischemic stroke

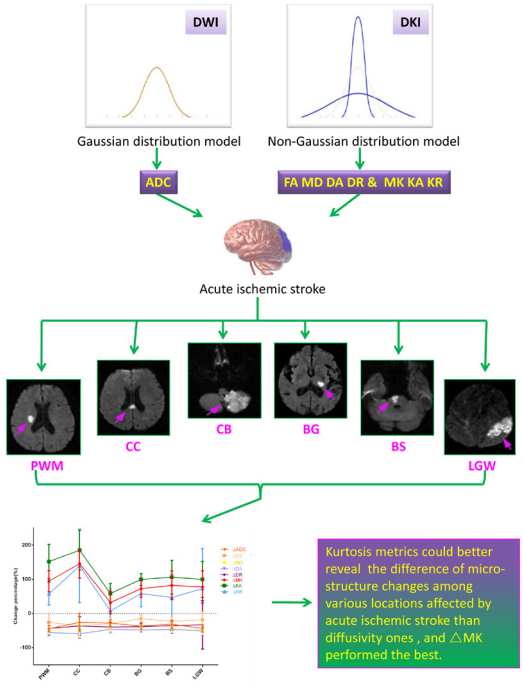

Correspondence to:
Gang Guo, MD,
guogangxm@163.com.

orcid:
0000-0003-1251-6744
(Liu-Hong Zhu)

doi: *10.4103/1673-5374.244791*

Received: *September 16, 2017*
Accepted: *June 12, 2018*

Abstract

The location of an acute ischemic stroke is associated with its prognosis. The widely used Gaussian model-based parameter, apparent diffusion coefficient (ADC), cannot reveal microstructural changes in different locations or the degree of infarction. This prospective observational study was reviewed and approved by the Institutional Review Board of Xiamen Second Hospital, China (approval No. 2014002). Diffusion kurtosis imaging (DKI) was used to detect 199 lesions in 156 patients with acute ischemic stroke (61 males and 95 females), mean age 63.15 ± 12.34 years. A total of 199 lesions were located in the periventricular white matter (n = 52), corpus callosum (n = 14), cerebellum (n = 29), basal ganglia and thalamus (n = 21), brainstem (n = 21) and gray-white matter junctions (n = 62). Percentage changes of apparent diffusion coefficient (ΔADC) and DKI-derived indices (fractional anisotropy [ΔFA], mean diffusivity [ΔMD], axial diffusivity [ΔD_a], radial diffusivity ΔD_r, mean kurtosis [ΔMK], axial kurtosis [ΔK_a], and radial kurtosis [ΔK_r]) of each lesion were computed relative to the normal contralateral region. The results showed that (1) there was no significant difference in ΔADC, ΔMD, ΔD_a or ΔD_r among almost all locations. (2) There was significant difference in ΔMK among almost all locations (except basal ganglia and thalamus *vs.* brain stem; basal ganglia and thalamus *vs.* gray-white matter junctions; and brainstem *vs.* gray-white matter junctions. (3) The degree of change in diffusional kurtosis in descending order was as follows: corpus callosum > periventricular white matter > brainstem > gray-white matter junctions > basal ganglia and thalamus > cerebellum. In conclusion, DKI could reveal the differences in microstructure changes among various locations affected by acute ischemic stroke, and performed better than diffusivity among all groups.

Key Words: *nerve regeneration; apparent diffusion coefficient; diffusion weighted imaging; diffusion kurtosis imaging; acute ischemic stroke; mean kurtosis; microstructure changes; white matter; 1.5 Tesla magnetic resonance system; neural regeneration*

Chinese Library Classification No. *R445; R741*

Introduction

Stroke, which has become the second leading cause of death among the global population aged > 60 years (Johnston et al., 2009; Thrift et al., 2014), has large impacts on patients and their families (Chen, 2008; Zhao et al., 2010; Liu et al., 2011). The incidence of ischemic stroke, a common form accounting for 43–79% of all strokes (Jia et al., 2010), is rising. Acute ischemic stroke, which is often fatal, is caused by thrombotic or embolic occlusion of a cerebral artery. Ischemia ensues, resulting in loss of neurological function (Writing Group Members et al., 2016; Khatri et al., 2018). Thrombolytic therapy is the treatment of choice for acute ischemic stroke if caught early enough (Yang et al., 2014; Liu and Zhang, 2017; Li et al., 2018b). The therapy is always based on the onset time reported by the patient or onlookers; however, few recognized radiological techniques can reveal whether there is recoverable tissue. (Domingues-Montanari et al., 2008). If the therapy timing is inappropriately late, complications such as cerebral hemorrhage and reperfusion injury may exacerbate tissue damage (Khatri et al., 2012; Kanazawa et al., 2017).

Studies have indicated that magnetic resonance imaging (MRI), especially diffusion imaging, has great potential in this field (Weber et al., 2015; Khalil et al., 2016; Piliszek et al., 2016; Li et al., 2018a). Diffusion weighted imaging (DWI) and its metric, the apparent diffusion coefficient (ADC), have played an important role in diagnosis and assessment of stroke since the 1990s (Sevick et al., 1990; Warach et al., 1992). Diffusion tensor imaging (DTI), a special kind of DWI based on the two-order 3D tensor model, is widely used to evaluate white matter changes in the brain (Basser et al., 1994; Auriel et al., 2014; Li et al., 2016). Both DWI and DTI are based on the fact that water molecules diffuse in a free and unrestricted environment (Basser and Jones, 2002). In biological tissues, an extremely complicated environment and structure affects water molecule diffusion, such that the diffusion displacement distribution occurs in a non-Gaussian form (Tuch et al., 2003). Several technologies, such as Q-space imaging (Assaf et al., 2002), diffusion spectrum imaging (Wedeen et al., 2005), and diffusion kurtosis imaging (DKI) (Jensen et al., 2005), have been proposed to characterize non-Gaussian diffusion patterns. Compared with similar approaches, DKI has the feature of being the least inconvenient in terms of scanning time and hardware demands.

DKI, proposed by Jensen et al. (2005), is a straightforward extension of diffusion tensor imaging. It uses a 2^{nd}-order diffusivity tensor together with a 4^{th}-order kurtosis tensor to provide an enhanced depiction of non-Gaussian water diffusion. Fieremans et al. (2011) and Hui et al. (2008) reported that DKI can detect subtle changes occurring in tissues affected by tumor or inflammation, and believed that DKI had great potential in the assessment of stroke lesions. Cheung et al. (2012) evaluated ischemic brain lesions using an animal model, and the results showed that DKI has great advantages in characterizing ischemic stroke. Whereas Rudrapatna et al. (2014) found that DKI could detect structural tissue changes and sensitively reflected angiogenesis and functional reconstruction around ischemic areas after the stroke occurred. The aim of our study was to evaluate the performance of DKI in detecting differences in microstructural changes at different locations of the brain after acute ischemic stroke.

Subjects and Methods

Subjects and design

This prospective observational study was reviewed and approved by the Institutional Review Board of Xiamen Second Hospital, China (approval No. 2014002). Written informed consent was obtained from all subjects before MRI. Inclusion criteria for subjects were as follows:

· Clinical symptoms, onset duration and neurological deficit symptoms of each subject were highly consistent with the diagnosis of acute ischemic stroke (Chung et al., 2014), and subjects did not undergo clinical treatment.

· This was the first onset for each subject.

· Cerebral hemorrhage or brain neoplasm were absent by brain computerized tomography (CT).

· There were no contraindications to MRI.

The exclusion criteria were:

· Patients could not finish the scanning.

· High signal intensity on DWI mapping and corresponding low signal on ADC mapping were not found.

· Maximum measurable lesion area was < 50 mm^2.

· There were artifacts that influenced the measurement.

One hundred sixty-eight patients (67 females and 101 males) aged 66.62 ± 14.88 years, with acute ischemic stroke, underwent routine MRI and DKI scans (b = 0, 1000, 2000 s/mm^2, 15 diffusion directions), were enrolled (**Figure 1**). Four patients with motion artifacts, six patients with maximum measurable lesion areas < 50 mm^2, and two patients with negative DWI and ADC were excluded. As a result, a total of 199 lesions were detected in the remaining 156 patients (61 females and 95 males) aged 63.15 ± 12.34 years. These lesions were divided into six groups according to commonly affected locations, including periventricular white matter (52 lesions), corpus callosum (14 lesions), cerebellum (29 lesions), basal ganglia and thalamus group (21 lesions), brainstem (21 lesions), and gray-white matter junctions (62 lesions) groups.

Data acquisition

Data acquisition was performed with a 1.5 T clinical MRI scanner (Signa HDe®, GE Medical System, Milwaukee, WI, USA) equipped with an eight-channel head and neck coil. Tight, but comfortable, foam padding was used to fix the head in place and minimize motion. Routine anatomical MRI sequences, including T1-weighted images (T1WI), T2-weighted images (T2WI), fluid attenuation inversion recovery T2WI, and DWI (b = 0, 1000 s/mm^2), were performed. DKI images were acquired using a spin-echo single-shot diffusion-weighted echo planar imaging sequence along 15 encoding diffusion directions at three b values (0, 1000, and 2000 s/mm^2). Scanning parameters were as follows: repetition time/echo time: 6000/162 ms; field of view: 24 cm × 24 cm; thickness/spacing: 5 mm/1.5 mm; number

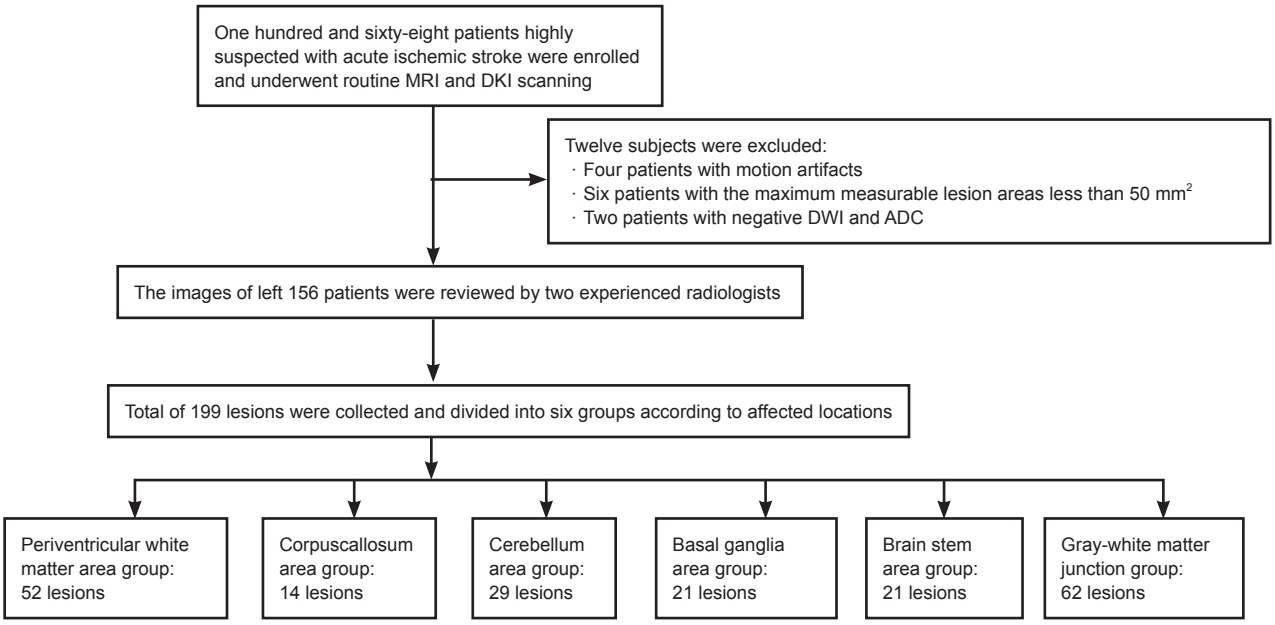

Figure 1 Flow chart of subject inclusion and grouping.

of excitations: 2; acquisition matrix: 96 × 130; total acquisition time was 6 minutes and 18 seconds. All metrics were obtained using DKI software on the Functool® platform of GE ADW4.3 workstation (GE Medical System).

For reliable results, we acquired these metrics in the following ways:

(i) Two experienced radiologists (FNW and QHC with 6 and 9 years of experience in stroke MR imaging, respectively) assessed the DKI-derived maps independently;

(ii) Each lesion was outlined on the diffusion-weighted image at b = 1000;

(iii) For each lesion, a mirrored contralateral normal region of interest (ROI) was placed;

(iv) The mean changes in percentages of all metrics in lesions with reference to the normal contralateral ROIs were computed using the measurements by the above two radiologists.

Mean values of ADC and DKI-derived metrics were measured. Percentage changes of all metrics (including apparent diffusion coefficient (ΔADC), fractional anisotropy [ΔFA], mean diffusivity [ΔMD], axial diffusivity [ΔD_a], radial diffusivity [ΔD_r], mean kurtosis [ΔMK], axial kurtosis [ΔK_a], and radial kurtosis [ΔK_r]) were computed relative to normal contralateral ROI using the formula:

$$\Delta METRIC = 100\% \times (METRIC_{affected} - METRIC_{normal}) / METRIC_{normal}. \quad (1)$$

Theoretical model of DWI

ADC is calculated according to Eq. 2, (Le Bihan et al., 1988; Gray and MacFall, 1998), where $S(b)$ and $S(b_0)$ represent the signal intensity at b and minimum-diffusion-weighted b_0. Typically, b_0 is set to zero and Eq. (1) can be rewritten as Eq. 3.

$$S(b) = S(b_0)e^{(b_0-b)ADC} \quad (2)$$

$$ADC = -\frac{\ln(S(b)/S(0))}{b} \quad (3)$$

Commonly, the value of b is set to 1000 s/mm^2 for the brain.

Theoretical model of DKI

DKI describes non-Gaussian water diffusion using a 2nd-order diffusion tensor together with a 4th-order kurtosis tensor. The diffusion-weighted signal $S(b)$ decays with increasing b value as the following equation (Le Bihan et al., 1986; Jensen et al., 2005; Jensen and Helpern, 2010):

$$\ln\frac{S(b)}{S(0)} = -bD_{app} + \frac{1}{6}b^2D_{app}^2K_{app} \quad (4)$$

where D_{app} is the apparent diffusion coefficient and K_{app} is the apparent diffusional kurtosis along the special direction. D_{app} and K_{app} along each direction are obtained by fitting diffusion-weighted signal intensities into Equation 4 with the least squares method. Diffusion tensor values and kurtosis tensor values can then be estimated using D_{app} and K_{app} along all directions. FA, MD, D_a, and D_r are derived from the diffusion tensor, while the diffusional kurtosis tensor is used to calculate MK, K_a, and K_r.

The value of MD is determined by D_{app} in all directions, while MK is determined by K_{app} in all directions. For example, the standard DKI sequence typically uses 15 directions and three b values (b = 0, 1000, 2000 s/cm^2) to collect data, and the calculation sketch map of MD and MK can be expressed as shown in **Figure 2**. **Figure 3** shows the DWI and DKI maps from a normal subject.

Statistical analysis

All statistical analyses were performed using commercial software (Statistical analysis software, SPSS® Version 19.0

for Windows; IBM SPSS, Chicago IL, USA). Mean values of all metrics were compared among different lesions. Meanwhile, Kolmogorov-Smirnov testing of ADCs and DKI-derived indices among metrics and groups were performed. Values of $P < 0.05$ were considered statistically significant.

Results

Comparison of DKI-derived metrics among six groups

Figures 4–9 show the DKI-derived indices within lesions in periventricular white matter, corpus callosum, cerebellum, basal ganglia and thalamus, brainstem, and gray-white matter junctions, respectively. As shown in **Figures 4**, **5**, and **8**, values of MD, D_a and D_r decreased substantially, while MK, K_a, and K_r increased markedly compared with the normal contralateral side. MK, K_a and K_r of lesions in the cerebellum (**Figure 6**) and gray-white matter junctions (**Figure 9**) demonstrated different patterns. Notably, only some lesions showed increased metrics as compared with the normal contralateral side. However, all diffusional kurtosis metrics were slightly increased in lesions of the basal ganglia and thalamus (**Figure 7**) compared with the normal contralateral side.

Comparison between ADC and DKI matrices among groups

As exhibited in **Figure 10,** as ADC and diffusivity metrics (FA, MD, D_a and D_r) decreased, and kurtosis metrics (MK, K_a and K_r) increased in all groups. In all groups, kurtosis metrics exhibited larger changes than ADC and diffusivity metrics, which indicated their potential in distinguishing differences among groups. Absolute percentage changes along the axial direction were significantly larger than along the radial direction in all groups: ΔD_a (−51.01 ± 10.77%) *vs.* ΔD_r (−37.55 ± 43.14%) ($P = 0.013$); ΔK_a (113.04 ± 57.14%) *vs.* ΔK_r (58.63 ± 85.36%) ($P = 0.002$).

Table 1 illustrates that there was no significant difference in ΔADC between almost all group pairings (except periventricular white matter *vs.* cerebellum; gray-white matter junction *vs.* cerebellum; $P > 0.05$); whereas there was a significant difference in ΔMK between almost all group pairings (except basal ganglia and thalamus *vs.* brain stem; basal ganglia and thalamus *vs.* lobes mixed with gray and white matter; and brain stem *vs.* lobes mixed with gray and white matter) ($P < 0.05$). Notably, ΔK_a performed almost the same as ΔMK, and there were no significant differences in ΔMD or ΔD_a between groups (except periventricular white matter *vs.* cerebellum; periventricular white matter *vs.* basal ganglia and thalamus) ($P > 0.05$). ΔD_r demonstrated no statistically significant changes among all groups ($P > 0.05$).

Discussion

Several previous studies found that the prognosis of stroke is dependent upon the location (Galovic et al., 2013; Phan et al., 2013; Tang et al., 2013). Moreover, researchers have long been looking for appropriate radiological parameters to describe the degree of infarction in specified locations. Although ADC is widely used in the clinic for diagnosis of acute and hyperacute ischemic stroke (Bevers et al., 2018; Nakajo et al., 2018), it cannot reveal microstructural changes in tissue or the degree of infarction. DWI assumes that water molecules diffuse in a free and non-restricted environment (Piliszek et al., 2016), while in tissues, water molecule diffusion is restricted by complicated microstructures and follows a non-Gaussian form of displacement distribution (Tuch et al., 2003).

In this study, we found that MD, D_a, and D_r obviously decreased in all groups, while MK, K_a, and K_r dramatically

Table 1 *P* value in Kolmogorov-Smirnov test of metrics among groups

	ΔADC	ΔFA	ΔMD	ΔD_a	ΔD_r	ΔMK	ΔK_a	ΔK_r
PWM *vs.* CC	0.948	0.353	0.549	0.479	0.734	0.033*	0.229	0.074
PWM *vs.* CB	<0.001*	0.557	0.013*	0.007*	0.405	< 0.001*	< 0.001*	< 0.001*
PWM *vs.* BG	0.135	0.002*	0.002*	0.002*	0.051	0.029*	0.002*	0.94
PWM *vs.* BS	0.28	0.281	0.07	0.061	0.07	0.024*	0.043*	0.043*
PWM *vs.* LGW	0.852	0.012*	0.285	0.064	0.882	0.001*	0.001*	0.032*
CC *vs.* CB	0.06	0.639	0.075	0.093	0.708	0.001*	0.001*	0.021*
CC *vs.* BG	0.534	0.009*	0.063	0.074	0.286	0.028*	0.028*	0.174
CC *vs.* BS	0.270	0.138	0.354	0.084	0.536	0.005*	0.049*	0.084
CC *vs.* LGW	0.941	0.126	0.4	0.126	0.769	0.007*	0.025*	0.111
CB *vs.* BG	0.066	0.051	0.956	0.663	0.61	0.001*	< 0.001*	0.003*
CB *vs.* BS	0.515	0.24	0.24	0.954	0.112	< 0.001*	0.006*	0.017*
CB *vs.* LGW	< 0.001*	0.202	0.077	0.227	0.162	0.001*	0.002*	0.014*
BG *vs.* BS	0.668	0.207	0.376	0.163	0.749	0.68	0.61	0.207
BG *vs.* LGW	0.367	0.214	0.054	0.165	0.053	0.452	0.219	0.214
BS *vs.* LGW	0.38	0.183	0.159	0.159	0.056	0.202	0.917	0.782

Value with the superscript character (*) in the table indicates that the *P* value was < 0.05. PWM: Periventricular white matter; CC: corpus callosum; CB: cerebellum; BG: basal ganglia and thalamus; BS: brain stem; LGW: gray-white matter junctions; ADC: apparent diffusion coefficient; FA: fractional anisotropy; MD: mean diffusivity; D_a: axial diffusivity; D_r: radial diffusivity; MK: mean kurtosis; K_a: axial kurtosis; K_r: radial kurtosis; DKI: diffusion kurtosis imaging.

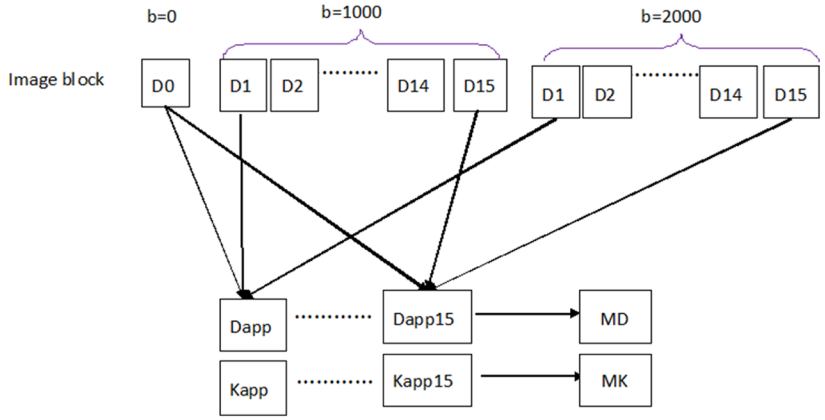

Figure 2 Calculation sketch map of MD and MK (DKI sequence using 15 directions and three *b* values typically).
The value of MD was decided by the values of D_{app} from all directions, K_{app} while the MK was decided by the values of from all directions. MD: Mean diffusivity; MK: mean kurtosis; DKI: diffusion kurtosis imaging.

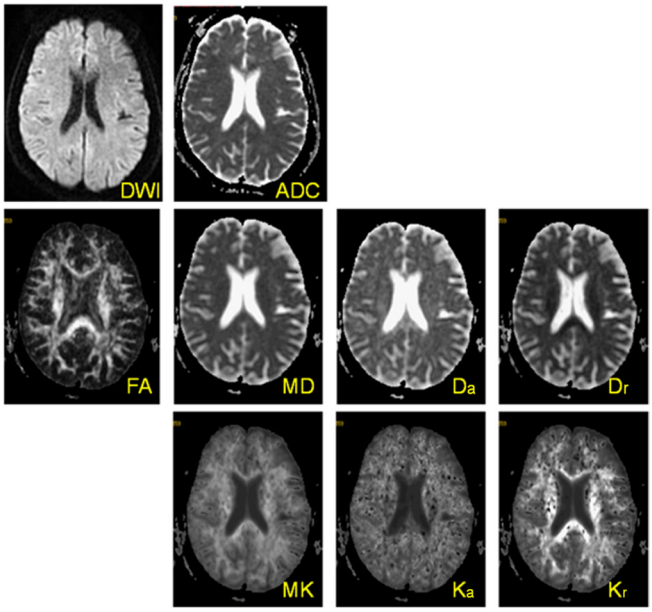

Figure 3 DWI and DKI metrics maps from a 46-year-old healthy female volunteer.
MD, D_a, and D_r maps were almost the same as the ADC map. DWI: Diffusion-weighted imaging; ADC: apparent diffusion coefficient; FA: fractional anisotropy; MD: mean diffusivity; D_a: axial diffusivity; D_r: radial diffusivity; MK: mean kurtosis; K_a: axial kurtosis; K_r: radial kurtosis; DKI: diffusion kurtosis imaging.

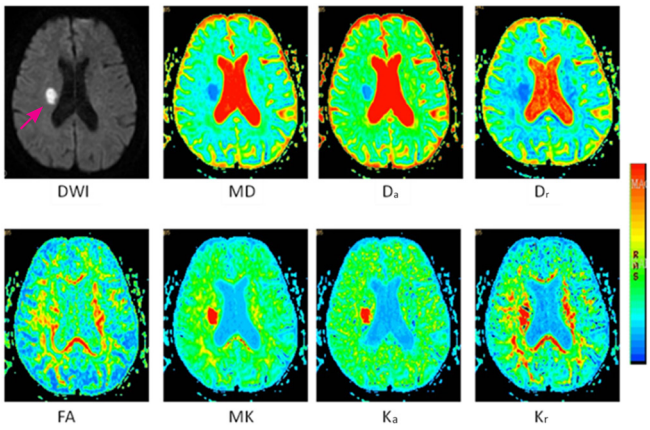

Figure 4 DKI-derived metric maps with lesion (pink arrow) located in periventricular white matter from a 73-year-old female patient suffering from an acute ischemic stroke (onset duration < 72 hours).
Signal intensity of the lesion is decreased markedly on MD, D_a, and D_r maps, while it is increased on MK, K_a, and K_r maps. DWI: Diffusion weighted imaging; MD: mean diffusivity; D_a: axial diffusivity; D_r: radial diffusivity; FA: fractional anisotropy; MK: mean kurtosis; K_a: axial kurtosis; K_r: radial kurtosis; DKI: diffusion kurtosis imaging.

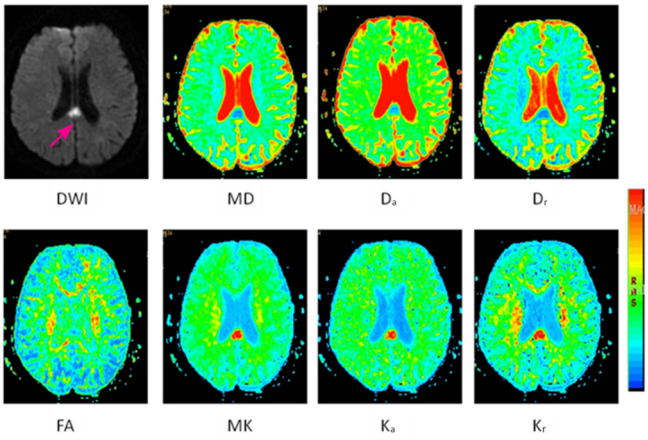

Figure 5 DKI-derived metric maps with a lesion (pink arrow) located in the corpus callosum from a 38-year-old female acute ischemic stroke patient (onset duration < 72 hours).
The signal intensity change of the lesion was the same as the lesion in the periventricular white matter area in Figure 4. DWI: Diffusion weighted imaging; MD: mean diffusivity; D_a: axial diffusivity; D_r: radial diffusivity; FA: fractional anisotropy; MK: mean kurtosis; K_a: axial kurtosis; K_r: radial kurtosis; DKI: diffusion kurtosis imaging.

increased in all groups. The behaviors of diffusion-derived parameters and kurtosis-derived parameters were quite different. In corpus callosum, periventricular white matter, and brainstem areas, diffusion-derived parameters decreased remarkably, while MK, K_a and K_r increased noticeably compared with the normal side. The kurtosis-derived parameters of lesions located in the basal ganglia and thalamus region increased slightly compared with the normal side. In lesions located at lobe areas mixed with gray and white matter, diffusion-derived parameters decreased slightly, with a corresponding slight increase in kurtosis-derived parameters. In lesions located in the cerebellum, diffusion-derived parameters decreased sharply, but the performances of MK, K_a, and K_r mapping were quite different from those of other locations; only parts of lesions increased in signal change

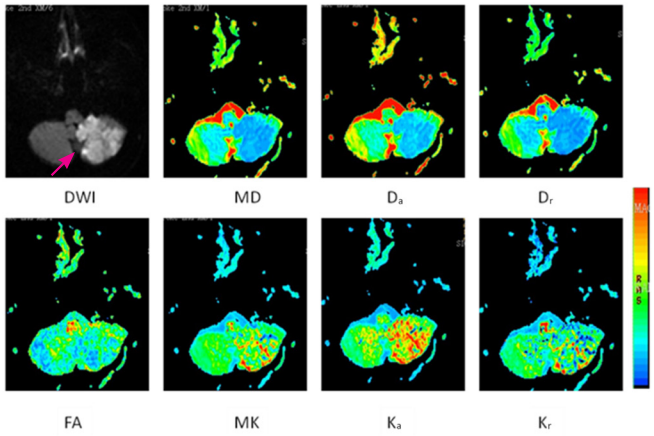

Figure 6 DKI-derived metric maps with lesion (pink arrow) involving the left cerebellar hemisphere from an 85-year-old male patient suffering from acute ischemic stroke (onset duration < 72 hours).
Signal intensity of the whole lesion decreased markedly on MD, D_a, and D_r maps, while part of the lesion's signal intensity was higher than its mirror normal side on MK, K_a, and K_r maps. DWI: Diffusion weighted imaging; MD: mean diffusivity; D_a: axial diffusivity; D_r: radial diffusivity; FA: fractional anisotropy; MK: mean kurtosis; K_a: axial kurtosis; K_r: radial kurtosis; DKI: diffusion kurtosis imaging.

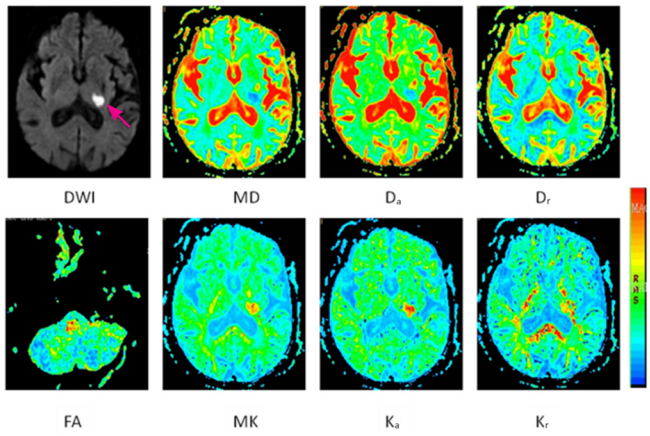

Figure 7 DKI-derived metric maps with focal lesion (pink arrow) located in the basal ganglia and thalamus from an 86-year-old female acute ischemic stroke patient (onset duration < 72 hours).
The signal intensity of the lesion was slightly higher than its mirror normal side on MK, K_a, and K_r maps. DWI: Diffusion weighted imaging; MD: mean diffusivity; D_a: axial diffusivity; D_r: radial diffusivity; FA: fractional anisotropy; MK: mean kurtosis; K_a: axial kurtosis; K_r: radial kurtosis; DKI: diffusion kurtosis imaging.

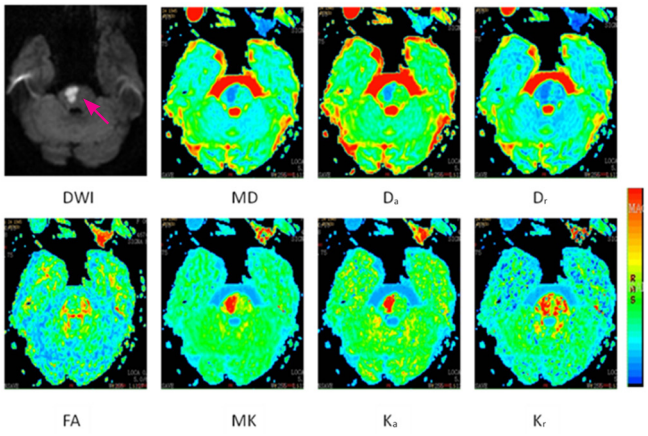

Figure 8 DKI-derived metric maps with lesion (pink arrow) involving the right half of the brainstem from a 69-year-old female patient suffering from acute ischemic stroke (onset duration < 72 hours).
The signal intensity change of the lesion was the same as the ones in the periventricular white matter (Figure 4) and corpus callosum (Figure 5) areas. DWI: Diffusion weighted imaging; MD: mean diffusivity; D_a: axial diffusivity; D_r: radial diffusivity; FA: fractional anisotropy; MK: mean kurtosis; K_a: axial kurtosis; K_r: radial kurtosis; DKI: diffusion kurtosis imaging.

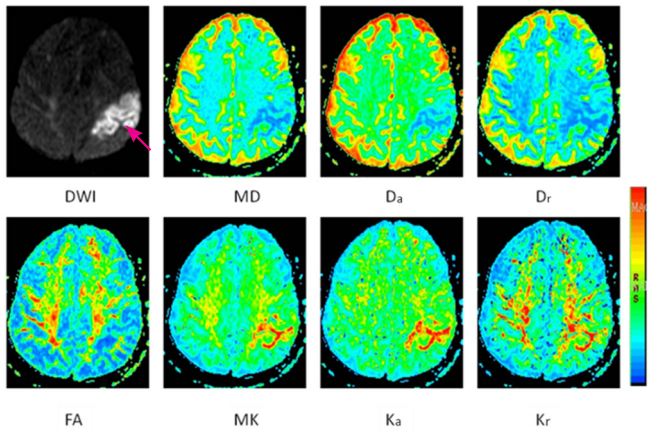

Figure 9 DKI-derived metric maps with lesion (pink arrow) located at parietooccipital lobe from a 60-year-old female acute ischemic stroke patient (onset duration < 72 hours).
Part of the lesion's signal intensity decreased on MD, D_a, and D_r maps, and increased on MK, K_a, and K_r maps correspondingly. DWI: Diffusion weighted imaging; MD: mean diffusivity; D_a: axial diffusivity; D_r: radial diffusivity; FA: fractional anisotropy; MK: mean kurtosis; K_a: axial kurtosis; K_r: radial kurtosis; DKI: diffusion kurtosis imaging.

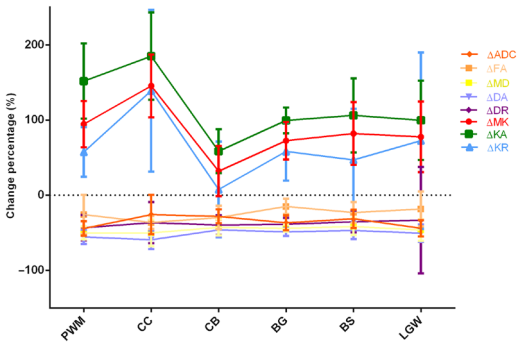

Figure 10 Comparison of ADC and DKI matrices among groups.
The upper three lines represent kurtosis-derived parameters, while the lower five lines represent the diffusion parameters. The upper three lines underwent larger changes, which meant that they had greater potential in distinguishing the differences among groups. PWM: Periventricular white matter; CC: corpus callosum; CB: cerebellum; BG: basal ganglia and thalamus; BS: brain stem; LGW: gray-white matter junctions; ADC: apparent diffusion coefficient; FA: fractional anisotropy; MD: mean diffusivity; D_a: axial diffusivity; D_r: radial diffusivity; MK: mean kurtosis; K_a: axial kurtosis; K_r: radial kurtosis; DKI: diffusion kurtosis imaging.

compared with the normal side. In descending order, changes in percentage of kurtosis-derived parameters (ΔMK and ΔK_a) in different locations was as follows: corpus callosum, periventricular white matter, brainstem, lobes mixed with gray and white matter, basal ganglia and thalamus, and cerebellum. This may indicate that when an acute ischemic stroke affects tissue mostly containing white matter, the microstructural changes of tissue are much more complex than those in other affected locations consisting of a higher proportion of gray matter.

As already known, the corpus callosum, brainstem, and periventricular white matter areas primarily contain white matter, while less white matter is found in lobes containing mixed gray and white matter. The basal ganglia and thalamus contain only gray matter. The cerebellum consists of a tightly folded layer of cortex with white matter underneath. These findings illustrate that in regions mostly containing white matter, the complexity of microstructural changes resulting from acute stroke is much higher than other affected regions, except the cerebellum. Although we have no distinct evidence to explain why affected tissue in the cerebellum performed quite differently from other regions, it should have some relationship with its microstructure.

In conclusion, when acute ischemic stroke affects tissues mostly containing white matter, the complexity of microstructural changes of the tissue is much higher than in other affected regions. DKI-derived kurtosis metrics, especially MK, have potential for characterizing different locations of brain tissue affected by acute ischemic stroke. Moreover, DKI technology can reveal differences in microstructural changes among different locations affected by acute ischemic stroke. For this purpose, kurtosis-derived parameters performed better than diffusivity-derived parameters.

Acknowledgments: *We are grateful for the support from Na Xu, Ye-Hua Song and Rui-Qiang Peng from the Department of Internal Neurology of Xiamen Second Hospital, China during patient recruitment and data acquisition.*

Author contributions: *Study design, data acquisition and analysis, work summarizing: LHZ; recruitment volunteers, data acquisition and outline lesions: QHC and FNW; algorithm and statistical analysis: ZPZ; study design and work supervising: GG. All authors approved the final version of the paper.*

Conflicts of interest: *The authors declare that there is no conflict of interests regarding the publication of this paper.*

Financial support: *This study was supported by the This study was supported by the Science and Technology Planned Project from Xiamen Science and Technology Bureau, China, No. 3502Z20154065 (to LHZ); the Joint Project for Xiamen Key Diseases from Xiamen Science and Technology Bureau, China, No. 3502Z20149032 (to GG). The funding bodies played no role in the study design, in the collection, analysis and interpretation of data, in the writing of the paper, or in the decision to submit the paper for publication.*

Institutional review board statement: *This study was approved by the Institutional Review Board of Xiamen Second Hospital, China (approval No. 2014002). The study was performed in accordance with the relevant laws and regulations of the Declaration of Helsinki, and the hospital's relevant ethical principles.*

Declaration of patient consent: *The authors certify that they have obtained all appropriate patient consent forms. In the form, patients have given their consent for their images and other clinical information to be reported in the journal. The patients understand that their names and initials will not be published and due efforts will be made to conceal their identity.*

Reporting statement: *This study followed the Standard Protocol Items: STrengthening the Reporting of OBservational studies in Epidemiology (STROBE) statement.*

Biostatistics statement: *The statistical methods of this study were reviewed by the biostatistician of Xiamen Second Hospital, China.*

Copyright license agreement: *The Copyright License Agreement has been signed by all authors before publication.*

Data sharing statement: *Individual participant data that underlie the results reported in this article, after deidentification (text, tables, figures, and appendices) will be in particular shared. Study protocol and informed consent form will be promulgated within 6 months after the completion of the trial. Anonymized trial data will be available indefinitely at www.figshare.com.*

Plagiarism check: *Checked twice by iThenticate.*

Peer review: *Externally peer reviewed.*

References

Assaf Y, Ben-Bashat D, Chapman J, Peled S, Biton IE, Kafri M, Segev Y, Hendler T, Korczyn AD, Graif M, Cohen Y (2002) High b-value q-space analyzed diffusion-weighted MRI: application to multiple sclerosis. Magn Reson Med 47:115-126.

Auriel E, Edlow BL, Reijmer YD, Fotiadis P, Ramirez-Martinez S, Ni J, Reed AK, Vashkevich A, Schwab K, Rosand J, Viswanathan A, Wu O, Gurol ME, Greenberg SM (2014) Microinfarct disruption of white matter structure: a longitudinal diffusion tensor analysis. Neurology 83:182-188.

Basser PJ, Jones DK (2002) Diffusion-tensor MRI: theory, experimental design and data analysis - a technical review. NMR Biomed 15:456-467.

Basser PJ, Mattiello J, LeBihan D (1994) MR diffusion tensor spectroscopy and imaging. Biophys J 66:259-267.

Bevers MB, Battey TWK, Ostwaldt AC, Jahan R, Saver JL, Kimberly WT, Kidwell CS (2018) Apparent diffusion coefficient signal intensity ratio predicts the effect of revascularization on ischemic cerebral edema. Cerebrovasc Dis 45:93-100.

Chen Z (2008) The mortality and death cause of national sample areas. In: The Third National Survey on the Cause of Death (Chen Z, ed), pp 14-15. Beijing: Peking Union Medical University Press.

Cheung JS, Wang E, Lo EH, Sun PZ (2012) Stratification of heterogeneous diffusion MRI ischemic lesion with kurtosis imaging: evaluation of mean diffusion and kurtosis MRI mismatch in an animal model of transient focal ischemia. Stroke 43:2252-2254.

Chung JW, Park SH, Kim N, Kim WJ, Park JH, Ko Y, Yang MH, Jang MS, Han MK, Jung C, Kim JH, Oh CW, Bae HJ (2014) Trial of ORG 10172 in Acute Stroke Treatment (TOAST) classification and vascular territory of ischemic stroke lesions diagnosed by diffusion-weighted imaging. J Am Heart Assoc 3:e001119.

Domingues-Montanari S, Mendioroz M, del Rio-Espinola A, Fernández-Cadenas I, Montaner J (2008) Genetics of stroke: a review of recent advances. Expert Rev Mol Diagn 8:495-513.

Fieremans E, Jensen JH, Helpern JA (2011) White matter characterization with diffusional kurtosis imaging. Neuroimage 58:177-188.

Galovic M, Leisi N, Muller M, Weber J, Abela E, Kagi G, Weder B (2013) Lesion location predicts transient and extended risk of aspiration after supratentorial ischemic stroke. Stroke 44:2760-2767.

Gray L, MacFall J (1998) Overview of diffusion imaging. Magn Reson Imaging Clin N Am 6:125-138.

Hui ES, Cheung MM, Qi L, Wu EX (2008) Towards better MR characterization of neural tissues using directional diffusion kurtosis analysis. Neuroimage 42:122-134.

Jensen JH, Helpern JA (2010) MRI quantification of non-Gaussian water diffusion by kurtosis analysis. NMR Biomed 23:698-710.

Jensen JH, Helpern JA, Ramani A, Lu H, Kaczynski K (2005) Diffusional kurtosis imaging: the quantification of non-gaussian water diffusion by means of magnetic resonance imaging. Magn Reson Med 53:1432-1440.

Jia Q, Liu LP, Wang YJ (2010) Stroke in China. Clin Exp Pharmacol Physiol 37:259-264.

Johnston SC, Mendis S, Mathers CD (2009) Global variation in stroke burden and mortality: estimates from monitoring, surveillance, and modelling. Lancet Neurol 8:345-354.

Kanazawa M, Takahashi T, Nishizawa M, Shimohata T (2017) Therapeutic strategies to attenuate hemorrhagic transformation after tissue plasminogen activator treatment for acute ischemic stroke. J Atheroscler Thromb 24:240-253.

Khalil AA, Hohenhaus M, Kunze C, Schmidt W, Brunecker P, Villringer K, Merboldt KD, Frahm J, Fiebach JB (2016) Sensitivity of diffusion-weighted STEAM MRI and EPI-DWI to infratentorial ischemic stroke. PLoS One 11:e0161416.

Khatri R, McKinney AM, Swenson B, Janardhan V (2012) Blood-brain barrier, reperfusion injury, and hemorrhagic transformation in acute ischemic stroke. Neurology 79:S52-57.

Khatri R, Vellipuram AR, Maud A, Cruz-Flores S, Rodriguez GJ (2018) Current endovascular approach to the management of acute ischemic stroke. Curr Cardiol Rep 20:46.

Le Bihan D, Breton E, Lallemand D, Grenier P, Cabanis E, Laval-Jeantet M (1986) MR imaging of intravoxel incoherent motions: application to diffusion and perfusion in neurologic disorders. Radiology 161:401-407.

Le Bihan D, Breton E, Lallemand D, Aubin ML, Vignaud J, Laval-Jeantet M (1988) Separation of diffusion and perfusion in intravoxel incoherent motion MR imaging. Radiology 168:497-505.

Li CC, Hao XZ, Tian JQ, Yao ZW, Feng XY, Yang YM (2018a) Predictors of short-term outcome in patients with acute middle cerebral artery occlusion: unsuitability of fluid-attenuated inversion recovery vascular hyperintensity scores. Neural Regen Res 13:69-76.

Li L, Sun G, Liu K, Li M, Li B, Qian SW, Yu LL (2016) White matter changes in posttraumatic stress disorder following mild traumatic brain injury: a prospective longitudinal diffusion tensor imaging study. Chin Med J (Engl) 129:1091-1099.

Li XY, Sun W, Yang Y, Zhang X, Li DM, Wang HZ, Sui XN, Chang H, Teng XH, Hu T, Zhang JB (2018b) Multimode computed tomography evaluation of the efficacy and safety of an extended thrombolysis time window (3–9 hours) for acute ischemic stroke: study protocol for a retrospective clinical trial based on medical records. Asia Pac J Clin Trials Nerv Syst Dis 3:43-52.

Liu J, Zhang GH (2017) Effect and mechanism of umbilical cord blood stem cells in the treatment of stroke. Zhongguo Zuzhi Gongcheng Yanjiu 21:1470-1476.

Liu L, Wang D, Wong KS, Wang Y (2011) Stroke and stroke care in China: huge burden, significant workload, and a national priority. Stroke 42:3651-3654.

Nakajo Y, Zhao Q, Enmi JI, Iida H, Takahashi JC, Kataoka H, Yamato K, Yanamoto H (2018) Early detection of cerebral infarction after focal ischemia using a new MRI indicator. Mol Neurobiol doi: 10.1007/s12035-018-1073-1.

Phan TG, Demchuk A, Srikanth V, Silver B, Patel SC, Barber PA, Levine SR, Hill MD (2013) Proof of concept study: relating infarct location to stroke disability in the NINDS rt-PA trial. Cerebrovasc Dis 35:560-565.

Piliszek A, Witkowski G, Sklinda K, Szary C, Ryglewicz D, Dorobek M, Walecki J (2016) Comprehensive imaging of stroke - Looking for the gold standard. Neurol Neurochir Pol 50:241-250.

Sevick RJ, Kucharczyk J, Mintorovitch J, Moseley ME, Derugin N, Norman D (1990) Diffusion-weighted MR imaging and T2-weighted MR imaging in acute cerebral ischaemia: comparison and correlation with histopathology. Acta Neurochir Suppl (Wien) 51:210-212.

Tang WK, Chen YK, Liang HJ, Chu WC, Mok VC, Ungvari GS, Wong KS (2013) Location of infarcts and apathy in ischemic stroke. Cerebrovasc Dis 35:566-571.

Thrift AG, Cadilhac DA, Thayabaranathan T, Howard G, Howard VJ, Rothwell PM, Donnan GA (2014) Global stroke statistics. Int J Stroke 9:6-18.

Tuch DS, Reese TG, Wiegell MR, Wedeen VJ (2003) Diffusion MRI of complex neural architecture. Neuron 40:885-895.

Umesh Rudrapatna S, Wieloch T, Beirup K, Ruscher K, Mol W, Yanev P, Leemans A, van der Toorn A, Dijkhuizen RM (2014) Can diffusion kurtosis imaging improve the sensitivity and specificity of detecting microstructural alterations in brain tissue chronically after experimental stroke? Comparisons with diffusion tensor imaging and histology. Neuroimage 97:363-373.

Warach S, Chien D, Li W, Ronthal M, Edelman RR (1992) Fast magnetic resonance diffusion-weighted imaging of acute human stroke. Neurology 42:1717-1723.

Weber RA, Hui ES, Jensen JH, Nie X, Falangola MF, Helpern JA, Adkins DL (2015) Diffusional kurtosis and diffusion tensor imaging reveal different time-sensitive stroke-induced microstructural changes. Stroke 46:545-550.

Wedeen VJ, Hagmann P, Tseng WY, Reese TG, Weisskoff RM (2005) Mapping complex tissue architecture with diffusion spectrum magnetic resonance imaging. Magn Reson Med 54:1377-1386.

Writing Group Members, Mozaffarian D, Benjamin EJ, Go AS, Arnett DK, Blaha MJ, Cushman M, Das SR, de Ferranti S, Despres JP, Fullerton HJ, Howard VJ, Huffman MD, Isasi CR, Jiménez MC, Judd SE, Kissela BM, Lichtman JH, Lisabeth LD, Liu S, et al. (2016) Executive Summary: Heart Disease and Stroke Statistics--2016 Update: A Report From the American Heart Association. Circulation 133:447-454.

Yang J, Zheng M, Chen S, Ou S, Zhang J, Wang N, Cao Y, Wang J (2014) Knowledge of thrombolytic therapy for acute ischemic stroke among community residents in western urban China. PLoS One 9:e107892.

Zhao Y, Yao Z, D'Souza W, Zhu C, Chun H, Zhuoga C, Zhang Q, Hu X, Zhou D (2010) An epidemiological survey of stroke in Lhasa, Tibet, China. Stroke 41:2739-2743.

C-Editor: Zhao M; S-Editors: Yu J, Li CH; L-Editors: Qiu Y, Song LP; T-Editor: Liu XL